Propagation of diffuse light in a turbid medium with multiple spherical inhomogeneities

Vitaliy N. Pustovit and Vadim A. Markel

We develop a fast and accurate solver for the forward problem of diffusion tomography in the case of several spherical inhomogeneities. The approach allows one to take into account multiple scattering of diffuse waves between different inhomogeneities. Theoretical results are illustrated with numerical examples; excellent numerical convergence and efficiency are demonstrated. The method is generalized for the case of additional planar diffuse–nondiffuse interfaces and is therefore applicable to the half-space and slab imaging geometries.

OCIS codes: 170.0170, 170.3660.

1. Introduction

Tomographic imaging methods utilizing nonionizing near-IR light have drawn continuously growing attention in recent years.[1] These methods are dramatically different from the conventional x-ray computerized tomography[2] owing to strong multiple scattering of the probing radiation inside the tissue. Indeed, propagation of the near-IR radiation in the so-called transparency window (700 nm $< \lambda <$ 900 nm) in most biological tissues is characterized by relatively weak absorption and strong scattering and is often described theoretically by the diffusion equation for the density of electromagnetic radiation.[3] The imaging modality based on detection of the multiply-scattered light has been referred to as diffusion tomography.

Obtaining tomographic images with the use of diffuse light requires one to solve an ill-posed inverse problem.[4] This ill-posedness is known to limit spatial resolution and quality of the obtained images. In addition, the inverse problem of the diffusion tomography is nonlinear.[4] Owing to the above circumstances, a significant effort has been devoted to optimizing instrumentation, data-collection schemes, and image-reconstruction algorithms with the ultimate goal of improving the quality and reliability of the obtained images (see, for example, Refs. 5–10). Often such optimization is done in numerical experiments with the use of mathematical phantoms. Numerical experiments are especially important for validation and optimization of the analytical image-reconstruction methods,[9–13] which utilize extremely large data sets. The use of mathematical phantoms requires, in turn, accurate forward solvers to generate numerical data for the inverse problem. The finite-difference and finite-element methods are general and allow one to generate data for phantoms of arbitrary shape. However, in three dimensions these methods can be exceedingly demanding computationally, and their accuracy is difficult to control. On the other hand, analytical forward solvers have been obtained so far only for mathematical phantoms in the shape of isolated spherical inhomogeneities.[14] It is clear that more complicated phantoms are required for evaluation of different image-reconstruction algorithms and data-collection schemes. Single spherical inhomogeneities can be especially inadequate for evaluating nonlinear image-reconstruction algorithms,[4,15] in which multiple scattering of diffuse waves can play an essential role. In this case, it is important to obtain accurate forward solvers for several inhomogeneities, including the effects of multiple scattering not only inside each inhomogeneity (as was done in Ref. 14) but also between different inhomogeneities.

In this paper we develop a semianalytical forward solver for the case of multiple interacting spherical

When this research was performed, the authors were with the Department of Radiology, Washington University, St. Louis, Missouri 63110. V. N. Pustovit is also with the Institute of Surface Chemistry, the National Academy of Sciences of Ukraine, 17 General Naumova Street, 03164 Kiev, Ukraine. V. A. Markel (v.markel@mail.med.upenn.edu) is now with the Department of Radiology, University of Pennsylvania, 3400 Spruce Street, 1 Silverstein, Philadelphia, Pennsylvania 19104.

Received 7 July 2003; revised manuscript received 15 September 2003; accepted 25 September 2003.

0003-6935/04/010104-09$15.00/0

inhomogeneities. More specifically, we obtain the data function in the form of an analytical expansion whose coefficients must be found numerically from a system of linear equations. Note that this system of equations, unlike the inverse problem of diffusion tomography, is well posed and therefore allows an accurate numerical solution. Note that the forward solver developed in this paper is inadequate for iterative image-reconstruction algorithms such as the functional Newton's method when the target is not known *a priori* and is not necessarily a collection of spheres. It is rather intended for accurate generation of forward data in numerical experiments with mathematical phantoms of spherical shape.

The problem of multiple scattering of electromagnetic waves from several interacting spherical particles was solved previously.[16–18] In this paper we extend the theoretical approach developed earlier for the Maxwell equations to the diffusion equation that describes propagation of diffuse waves. Note that slow convergence of solutions can be a major problem in the electromagnetic case. Indeed, obtaining accurate solutions for touching spheres with a metallike dielectric function requires extremely high-order expansion coefficients and is therefore computationally ineffective, if at all possible.[19] However, in the case of diffusing waves, the convergence is much faster even for high-contrast touching spherical inhomogeneities (high contrast of the inhomogeneities with respect to the background is the mathematical analog of the large dielectric function of metals in the electromagnetic case).

The paper is organized as follows. In Section 2 we develop the theoretical formalism for scattering of diffuse waves from multiple spherical inhomogeneities embedded in an infinite macroscopically homogeneous medium. Numerical examples are given in Section 3. In Section 4 we generalize the theoretical approach to the case in which the scattering medium is not infinite (either a half-space or a slab) and consider additional boundary conditions on diffuse–nondiffuse interfaces. Finally, Section 5 contains a summary of obtained results.

2. Theoretical Model

We start with the description of the theoretical model. The fundamental assumption of this paper is that the energy density of diffuse light $u(\mathbf{r}, t)$ produced by a spatially and time-varying source $S(\mathbf{r}, t)$ obeys the diffusion equation

$$\frac{\partial u(\mathbf{r}, t)}{\partial t} = \nabla \cdot [D(\mathbf{r})\nabla u(\mathbf{r}, t)] - \alpha(\mathbf{r})u(\mathbf{r}, t) + S(\mathbf{r}, t), \tag{1}$$

where $\alpha(\mathbf{r})$ and $D(\mathbf{r})$ are the position-dependent absorption and diffusion coefficients. Note that α and D are related to the scattering and absorption coefficients μ_a and μ_s, which are commonly encountered in the radiative transfer theory by $\alpha = c\mu_a$ and $D = c/\{3[\mu_a + (1 - g)\mu_s]\}$, where c is the average velocity of light in the medium and g is the asymmetry factor. Thus α has units of frequency, and D has units of area per unit time. We further assume that $\alpha(\mathbf{r})$ and $D(\mathbf{r})$ are piecewise constant, i.e.,

$$\alpha(\mathbf{r}) = \begin{cases} \bar{\alpha}, & \mathbf{r} \notin \bigcup_{i=1}^{N} V_i \\ \alpha_i, & \mathbf{r} \in V_i \end{cases}, \tag{2}$$

$$D(\mathbf{r}) = \begin{cases} \bar{D}, & \mathbf{r} \notin \bigcup_{i=1}^{N} V_i \\ D_i, & \mathbf{r} \in V_i \end{cases}. \tag{3}$$

Here V_i, $i = 1, \ldots, N$, are spherical regions defined by $|\mathbf{r} - \mathbf{r}_i| < a_i$, where $\mathbf{r}_i$ and a_i are the radius vector of the center and the radius of the spherical region V_i, respectively, $\bar{\alpha}$ and $\bar{D}$ are the background values of the absorption and diffusion coefficients, and α_i and D_i are the respective values inside the ith spherical region.

In most practical applications, the source of diffuse radiation is located outside the area where the optical coefficients are inhomogeneous and is harmonically amplitude modulated according to $S(\mathbf{r}, t) = S(\mathbf{r})[1 + A \exp(-i\omega t)]$, where $A < 1$. [Continuous-wave (cw) imaging corresponds to the case $A = 0$.] Then everywhere in space, except for the surfaces of discontinuity of α and D, Eq. (1) takes the form

$$[\nabla^2 - k^2(\mathbf{r})]u(\mathbf{r}) = -\frac{1}{\bar{D}} S(\mathbf{r}), \tag{4}$$

where $u(\mathbf{r})$ is the Fourier component of $u(\mathbf{r}, t)$ oscillating at the frequency ω and the (generally, complex) diffuse wave number $k(\mathbf{r})$ is also piecewise constant and given by

$$k(\mathbf{r}) = \left[\frac{\alpha(\mathbf{r}) - i\omega}{D(\mathbf{r})}\right]^{1/2} = \begin{cases} \bar{k}, & \mathbf{r} \notin \bigcup_{i=1}^{N} V_i \\ k_i, & \mathbf{r} \in V_i \end{cases}, \tag{5}$$

where

$$\bar{k} = \left(\frac{\bar{\alpha} - i\omega}{\bar{D}}\right)^{1/2}, \qquad k_i = \left(\frac{\alpha_i - i\omega}{D_i}\right)^{1/2}. \tag{6}$$

In addition, on the surfaces of discontinuity $|\mathbf{r} - \mathbf{r}_i| = a_i$, the following boundary conditions must be satisfied[20]:

$$u|_{\mathbf{r}=\mathbf{r}_i+(a_i-\epsilon)\hat{\mathbf{n}}} = u|_{\mathbf{r}=\mathbf{r}_i+(a_i+\epsilon)\hat{\mathbf{n}}}, \tag{7}$$

$$D_i\hat{\mathbf{n}} \cdot \nabla u|_{\mathbf{r}=\mathbf{r}_i+(a_i-\epsilon)\hat{\mathbf{n}}} = \bar{D}\hat{\mathbf{n}} \cdot \nabla u|_{\mathbf{r}=\mathbf{r}_i+(a_i+\epsilon)\hat{\mathbf{n}}}, \tag{8}$$

where ϵ is an infinitesimally small constant and $\hat{\mathbf{n}}$ is an arbitrary unit vector. The first equation expresses continuity of the field $u(\mathbf{r})$ across the interfaces, and the second equation expresses continuity of the normal component of the flux.

Because point sources are most often used in diffusion tomography, we will obtain the solution to Eq. (4) for a point source of the form $S(\mathbf{r}) = S_0\delta(\mathbf{r} - \mathbf{r}_s)$, where $\mathbf{r}_s$ is the location of the source. More general solutions can be easily obtained by superposition. The geometry of the problem is illustrated in Fig. 1.

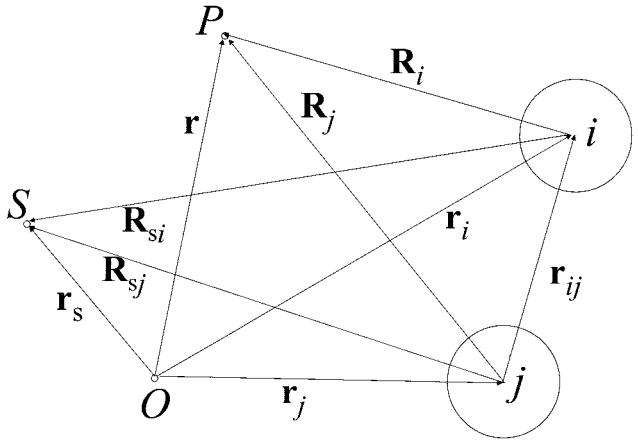

Fig. 1. Sketch of the problem geometry and graphical illustration of the definitions of vectors $\mathbf{R}_i$ and $\mathbf{R}_{si}$ and $\mathbf{r}_{ij}$. The source (S), the point of observation (P), the center of laboratory reference frame (O), and two spheres are shown.

For an arbitrary point P characterized by the radius vector $\mathbf{r}$, we introduce the notation $\mathbf{R}_i = \mathbf{r} - \mathbf{r}_i$. We also denote the vector drawn from the center of the ith sphere to the source as $\mathbf{R}_{si} = \mathbf{r}_s - \mathbf{r}_i$.

Now we briefly outline the method for matching the boundary conditions on the surfaces of discontinuity. The approach described below is based on translation of scalar spherical harmonics and is analogous to the one used in the electromagnetic theory. There are, however, substantial differences. Most importantly, unlike the propagating electromagnetic waves, the diffuse waves are exponentially decaying.[3] Second, the diffuse waves are scalar. In the electromagnetic case, expansion of the electric field inside a sphere into vector spherical harmonics starts from the order $l = 1$. However, expansion of the field u inside a sphere into the scalar spherical harmonics starts from the order $l = 0$. This fact changes the nature of the dipole approximation as it may be applied to the multiple scattering of diffuse waves. Last, the field $u(\mathbf{r}, t)$ has the physical meaning of the energy density and is therefore strictly positive. This fact puts certain restrictions on the expansion coefficients introduced below. Note that these restrictions are not present in the electromagnetic case.

The field inside the ith sphere must satisfy Eq. (4) with $k(\mathbf{r}) = k_i$ and be finite everywhere inside the sphere. Therefore it can be expanded as

$$u(\mathbf{r}) = \sum_{l=0}^{\infty} \sum_{m=-l}^{l} A_{ilm} i_l(k_i R_i) Y_{lm}(\hat{\mathbf{R}}_i), \qquad R_i < a_i. \quad (9)$$

Here A_{ilm} are unknown coefficients, $i_l(x) = i^{-1} j_l(ix)$ are the modified spherical Bessel functions of the first kind, and $Y_{lm}(\hat{\mathbf{R}}_i)$ are the spherical functions defined by the direction of the unit vector $\hat{\mathbf{R}}_i = \mathbf{R}_i/R_i$ in the laboratory frame. Outside the spherical regions V_i, the field is given by a superposition of the incident field $u_0(\mathbf{r})$ (which is equal to the field produced by the source in an infinite homogeneous medium) and the scattered field $u_s(\mathbf{r})$:

$$u(\mathbf{r}) = u_0(\mathbf{r}) + u_s(\mathbf{r}), \qquad \mathbf{r} \notin \bigcup_{i=1}^{N} V_i. \quad (10)$$

The incident field is given by

$$\begin{aligned} u_0(\mathbf{r}) &= \frac{S_0 \exp(-\bar{k}|\mathbf{r} - \mathbf{r}_s|)}{4\pi \bar{D} |\mathbf{r} - \mathbf{r}_s|} \\ &= \frac{S_0 \exp(-\bar{k}|\mathbf{R}_i - \mathbf{R}_{si}|)}{4\pi \bar{D} |\mathbf{R}_i - \mathbf{R}_{si}|} \\ &= \sum_{l=0}^{\infty} \sum_{m=-l}^{l} B_{ilm}^{(0)} i_l(\bar{k} R_i) Y_{lm}(\hat{\mathbf{R}}_i), \qquad \forall\, i, \end{aligned} \quad (11)$$

where

$$B_{ilm}^{(0)} = \frac{S_0 \bar{k}}{\bar{D}} k_l(\bar{k} R_{si}) Y_{lm}^*(\hat{\mathbf{R}}_{si}) \quad (12)$$

and $k_l(x) = -i^l h_l^{(1)}(ix)$ is the modified spherical Hankel function of the first kind (defined without the $\pi/2$ factor). The last equality in Eq. (11) was obtained by expansion of a spherical wave into spherical harmonics with the additional condition $R_i < R_{si}$. This inequality is valid in a sufficiently close vicinity of the surface of any sphere, provided that the source is separated from this surface by a finite distance. Because we will use only Eqs. (11) and (12) to satisfy boundary conditions on the surfaces of discontinuity, we do not need to consider the case $R_i > R_{si}$. Note also that the sum in the right-hand side of Eq. (11) does not depend on the number of the spherical inhomogeneity, i, even though individual terms depend on this index. Thus expansion (11) with coefficients given by Eq. (12) is valid for any value of i. A specific representation (for a given value of i) will be used to satisfy the boundary conditions on the surface of the ith sphere.

The scattered fields $u_s(\mathbf{r})$ are a superposition of fields scattered by all spherical inhomogeneities:

$$u_s(\mathbf{r}) = \sum_{i=1}^{N} u_{si}(\mathbf{r}). \quad (13)$$

The functions $u_{si}(\mathbf{r})$ can be, in turn, expanded as

$$u_{si}(\mathbf{r}) = \sum_{l=0}^{\infty} \sum_{m=-l}^{l} B_{ilm} k_l(\bar{k} R_i) Y_{lm}(\hat{\mathbf{R}}_i), \quad (14)$$

where B_{ilm} is another set of unknown coefficients.

We seek to satisfy boundary conditions (7) and (8) on the surface of each sphere. Let us consider the ith sphere and write the scattered field in the vicinity of its surface as

$$u_s(\mathbf{r}) = u_{si}(\mathbf{r}) + \sum_{j \neq i} u_{sj}(\mathbf{r}). \quad (15)$$

Thus we have separated the field scattered by the ith sphere from the input of all other spheres. Next, we

use the following formula for translation of scalar spherical harmonics[21]:

$$k_l(\bar{k}R_j)Y_{lm}(\hat{\mathbf{R}}_j) = \sum_{l=0}^{\infty}\sum_{m=-l}^{l} K_{lm}^{l'm'}(\mathbf{r}_{ij}) i_{l'}(\bar{k}R_i) Y_{l'm'}(\hat{\mathbf{R}}_i), \tag{16}$$

where

$$K_{lm}^{l'm'}(\mathbf{r}_{ij}) = 4\pi(-1)^{l'} \sum_{l''=|l'-l|}^{|l'+l|} \Gamma_{l',m'}^{l,m,l'',m-m'} \mathcal{H}_{l''}(\bar{k}r_{ij}) \times Y_{l'',m-m'}(\hat{\mathbf{r}}_{ij}) \tag{17}$$

and $\mathbf{r}_{ij} = \mathbf{r}_i - \mathbf{r}_j$ and the coefficients $\Gamma_{l',m'}^{l,m,l'',m''}$ are expressed in terms of the Wigner three-j symbols

$$\begin{pmatrix} j_1 & j_2 & j_3 \\ m_1 & m_2 & m_3 \end{pmatrix}$$

as

$$\Gamma_{l',m'}^{l,m,l''m''} = (-1)^m \left[\frac{(2l+1)(2l'+1)(2l''+1)}{4\pi}\right]^{1/2} \times \begin{pmatrix} l & l' & l'' \\ 0 & 0 & 0 \end{pmatrix} \begin{pmatrix} l & l' & l'' \\ -m & m' & m'' \end{pmatrix}. \tag{18}$$

Rearranging indexes, we can write the total external field in the vicinity of the ith sphere as

$$\begin{aligned} u(\mathbf{r}) = &\sum_{l=0}^{\infty}\sum_{m=-l}^{l} B_{ilm}^{(0)} i_l(\bar{k}R_i) Y_{lm}(\hat{\mathbf{R}}_i) \\ &+ \sum_{l=0}^{\infty}\sum_{m=-l}^{l} B_{ilm} k_l(\bar{k}R_i) Y_{lm}(\hat{\mathbf{R}}_i) \\ &+ \sum_{j\neq i}\sum_{l=0}^{\infty}\sum_{m=-l}^{l} i_l(\bar{k}R_i) Y_{lm}(\hat{\mathbf{R}}_i) \\ &\times \sum_{l'=0}^{\infty}\sum_{m'=-l'}^{l'} K_{l'm'}^{lm}(\mathbf{r}_{ij}) B_{jl'm'}. \end{aligned} \tag{19}$$

Now we substitute expressions (9) and (19) for the internal and external fields near the surface of the ith sphere into boundary conditions (7) and (8). This results in a system of linear equations with respect to the unknown coefficients A_{ilm} and B_{ilm}:

$$A_{ilm} i_l(k_i a_i) = i_l(\bar{k}a_i)\left[B_{ilm}^{(0)} + \sum_{j\neq i}\sum_{l'=0}^{\infty}\sum_{m'=-l'}^{l'} K_{l'm'}^{lm}(\mathbf{r}_{ij}) \times B_{jl'm'}\right] + k_l(\bar{k}a_i) B_{ilm}, \tag{20}$$

$$D_i k_i A_{ilm} i_l'(k_i a_i) = \bar{D}\bar{k}\left\{i_l'(\bar{k}a_i)\left[B_{ilm}^{(0)} + \sum_{j\neq i}\sum_{l'=0}^{\infty}\sum_{m'=-l'}^{l'} \times K_{l'm'}^{lm}(\mathbf{r}_{ij}) B_{jl'm'}\right] + k_l'(\bar{k}a_i) B_{ilm}\right\}. \tag{21}$$

Here primes denote derivatives of the Bessel and Hankel functions. We can eliminate the internal field coefficients A_{ilm} from Eqs. (20) and (21) to obtain a system of equations of reduced size with respect to the external field coefficients B_{ilm}, which has the form

$$\frac{B_{ilm}}{\beta_{il}} + \sum_{j\neq i}\sum_{l'=0}^{\infty}\sum_{m'=-l'}^{l'} K_{lm}^{l'm'}(\mathbf{r}_{ij}) B_{jl'm'} = -B_{ilm}^{(0)}, \tag{22}$$

where

$$\beta_{il} = \frac{D_i k_i i_l(\bar{k}a_i) i_l'(k_i a_i) - \bar{D}\bar{k} i_l(k_i a_i) i_l'(\bar{k}a_i)}{D_i k_i i_l'(k_i a_i) k_l(\bar{k}a_i) - \bar{D}\bar{k} i_l(k_i a_i) k_l'(\bar{k}a_i)}. \tag{23}$$

In particular, in the limit $\mathbf{r}_{ij} \to \infty$ (noninteracting limit) the second term in Eq. (22) may be omitted, and we obtain $B_{ilm} = -\beta_{il} B_{ilm}^{(0)}$, which is the standard scalar Mie solution.

The system of equations can be written compactly as $\sum_{jl'm'} W_{ilm}^{jl'm'} B_{jl'm'} = -B_{ilm}^{(0)}$. In the cw case, the matrix W is Hermitian, i.e., $W_{ilm}^{jl'm'} = (W_{jl'm'}^{ilm})^*$. However, for a finite modulation frequency ω, it is neither Hermitian nor symmetrical. Instead, the following symmetry property is fulfilled: $W_{ilm}^{jl'm'}(\omega) = [W_{jl'm'}^{ilm}(-\omega)]^*$.

The quantity of interest in diffusion tomography is not $u(\mathbf{r})$ but the scattered field $u_s(\mathbf{r})$ or, more specifically, the quantity

$$\Delta I(\mathbf{r}) = \frac{c}{4\pi}[u_0(\mathbf{r}) - u(\mathbf{r})] = -\frac{c}{4\pi} u_s(\mathbf{r}). \tag{24}$$

Here $c = c_0/n$ is the average speed of light in the medium (c_0 is the speed of light in vacuum, and n is the average refractive index of the medium), and the factor $c/4\pi$ is introduced to relate the density of electromagnetic energy $u(\mathbf{r})$ to the physically measurable energy flux $I(\mathbf{r})$. The quantity $\Delta I(\mathbf{r})$ in the left-hand side of Eq. (24) is the change in the flux due to the presence of inhomogeneities. This quantity is usually referred to as the data function. It can be calculated at any point in space by use of Eqs. (13) and (14), where the coefficients B_{ilm} must be found from the system of Eqs. (22). The latter is a system of infinite size and must be truncated in any numerical calculation at some maximum value $l = l_{\max}$. The number of equations in the truncated system is $N(l_{\max}+1)^2$. One may assume that the convergence is reached when the function $u_s(\mathbf{r})$ does not change substantially when $l_{\max}$ is further increased.

Once the external field coefficients are found, the internal field coefficients can be calculated by use of the formula

$$A_{ilm} = -B_{ilm} \frac{\bar{D}/\bar{k}a_i^2}{D_i k_i i_l(\bar{k}a_i) i_l'(k_i a_i) - \bar{D}\bar{k} i_l(k_i a_i) i_l'(\bar{k}a_i)}, \tag{25}$$

which follows directly from the system of Eqs. (20) and (21) and the Wronskian relations for the modified Bessel and Hankel functions.

3. Numerical Simulations

We now illustrate the theoretical results obtained above with numerical simulations of the data func-

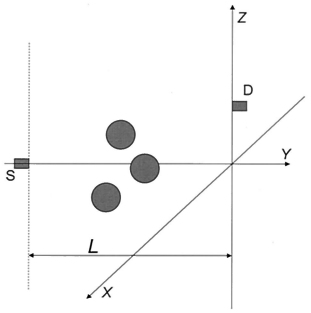

Fig. 2. Sketch of the data-collection scheme. The position of the source is fixed with respect to the inhomogeneities, and the detector is scanned on the Z axis. The distance between the source and the Z axis is $L = \lambda_{\mathrm{diff}} \equiv 2\pi/\bar{k}$.

tion (24) for different numbers and arrangements of spherical inhomogeneities. We consider the cw case ($\omega = 0$), so that the values of k_i and $\bar{k}$ are purely real. We also assume that all the spheres are of the same radius $a_i = a \ \forall \ i$ and that the inhomogeneities are purely absorbing, namely, $D_i = \bar{D} \ \forall \ i$. First, we consider strongly absorbing inhomogeneities with $\alpha_i = 16\bar{\alpha} \ \forall \ i$; correspondingly, $k_i = 4\bar{k} \ \forall \ i$. It can be easily verified that, if $\alpha_i > \bar{\alpha} \ \forall \ i$ and $D_i = \bar{D} \ \forall \ i$, the

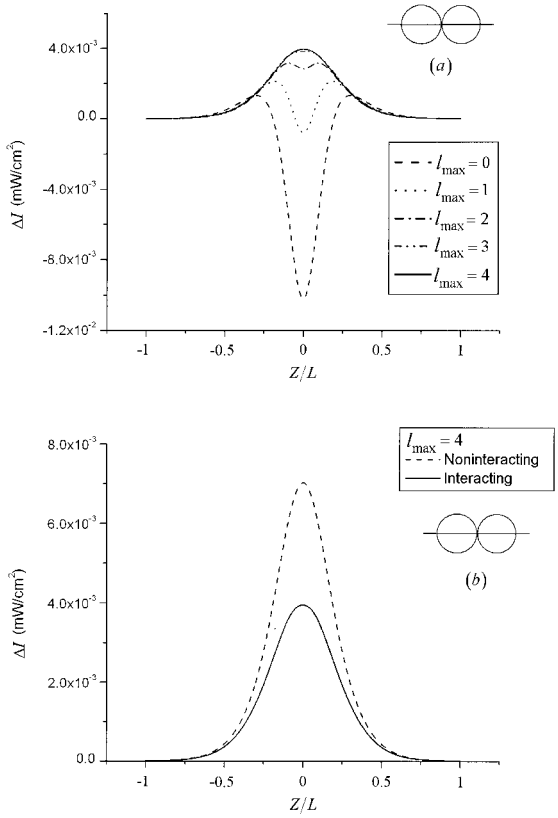

Fig. 3. Data function ΔI calculated as a function of the detector position Z for two touching spheres with radii $a = 0.2L$ and centers at (0, $0.3L$, 0) and (0, $0.7L$, 0) for the intensity of the source $S_0 = 100$ mW and $k_1 = k_2 = 4\bar{k}$. (a) Convergence of the solution with $l_{\max}$, and (b) comparison of the fully converged result with the noninteracting approximation for the same value of $l_{\max}$.

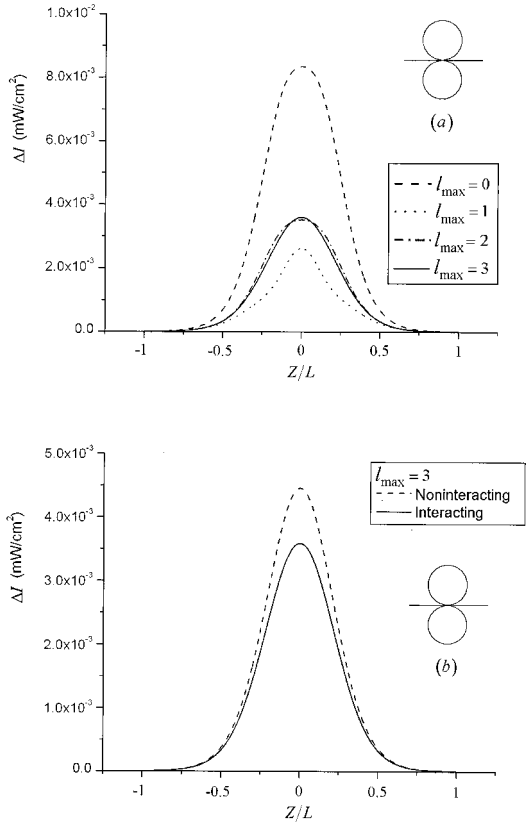

Fig. 4. Same as in Fig. 3 but for two touching spheres with radii $a = 0.2L$ and centers at (0, $0.5L$, $0.2L$) and (0, $0.5L$, $-0.2L$).

data function (24) is strictly positive. Further, we have selected the following values of the background coefficients: $\bar{\alpha} = 1$ GHz and $\bar{D} = 1$ cm^2/ns, which correspond to the typical values in biological tissues. The corresponding background diffuse wave number is $\bar{k} = 1$ cm^{-1}. The average speed of light in the medium is chosen to be $c = 2.26 \times 10^{10}$ cm/s, which corresponds to the refraction index of water ($n = 1.33$). We have also chosen the intensity of the source to be $S_0 = 100$ mW, and the data function is displayed in physical units (milliwatts per square centimeter). The geometry of the measurements is shown in Fig. 2. Here the source is fixed with respect to the inhomogeneities, and the detector is scanned in the plane separated from the source by the distance $L = \bar{\lambda}_{\mathrm{diff}} \equiv 2\pi/\bar{k}$, where $\bar{\lambda}_{\mathrm{diff}}$ is the diffuse wavelength.

The results for two touching spheres of the radius $a = 0.2L$ whose centers are placed along and perpendicular to the Y axis are shown in Figs. 3 and 4, respectively. In the top panels [Figs. 3(a) and 4(a)] the convergence of the data function with $l_{\max}$ is illustrated. We note that the fully converged results are strictly positive, as expected. The bottom panels [Figs. 3(b) and 4(b)] show the effect of intersphere multiple scattering. Namely, we compare the fully converged data function (solid curves) for two spheres with the data function obtained for the same value of $l_{\max}$ when the interaction term in Eq. (22) is neglected

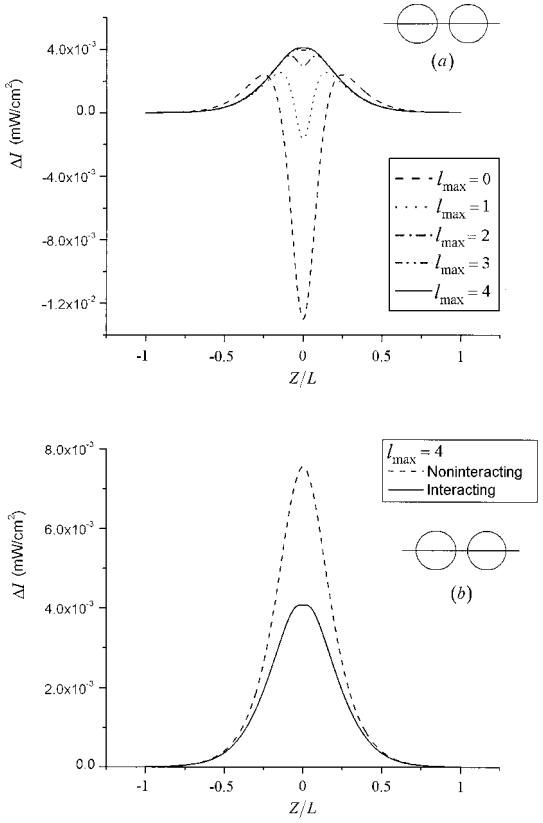

Fig. 5. Same as in Fig. 3 but for two nontouching spheres with radii $a = 0.2L$ and centers at (0, $0.3L$, 0) and (0, $0.8L$, 0).

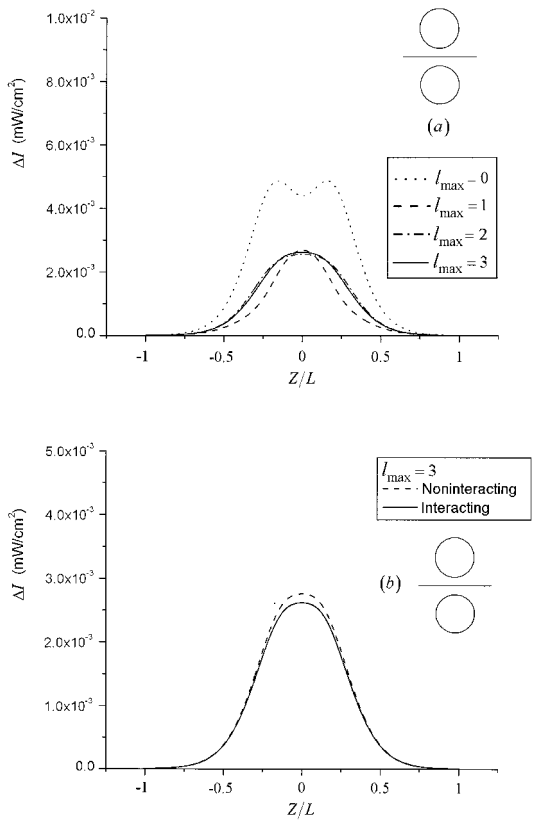

Fig. 6. Same as in Fig. 4 but for two nontouching spheres with radii $a = 0.2L$ and centers at (0, $0.5L$, $0.3L$) and (0, $0.5L$, $-0.3L$).

(dashed curves). First, we note that, even though the spheres are touching and the contrast between the optical properties of the spheres and the background is high, convergence is reached for relatively low values of l_{max} ($l_{max} \approx 4$). This value of l_{max} is close to the diffraction parameter of an isolated sphere, $x = k_i a = 4\bar{k}a \approx 5$. It should be noted that, in the case of electromagnetic scattering from touching spheres, the value of l_{max} required for convergence is, typically, much larger than x.[22] This is explained by the fact that secondary waves scattered by a given sphere are highly inhomogeneous inside neighboring spheres and must therefore excite spherical harmonics of high order.[19] This fact was demonstrated both numerically[19] and experimentally.[24] We believe that the reason we obtain this fast convergence (compared with the electromagnetic case) is that the free-space Green's function for the scalar diffusion equations decays as $1/r$ at small distances, whereas the Green's function for the Maxwell equations (for the electric field rather than the vector potential) decays as $1/r^3$ and therefore varies much stronger in space.[25] Second, it is obvious that the interaction of spheres is much stronger when the centers of the spheres are located on the Y axis. This is explained by the fact that in this case the sphere that is closer to the detector is located in the shadow of the other sphere. It can be seen that the result obtained in the noninteracting representation is severely inaccurate because it exceeds the maximum possible value of $\Delta I_{max} \approx 5.6 \times 10^{-3}$ mW/cm^2, which corresponds to total absence of diffuse radiation at the point Z = 0. In the case in which the centers of the spheres are on a line that is perpendicular to the Y axis (Fig. 4), the effects of intersphere multiple scattering are much weaker.

The results for two nontouching spheres of the same radius and contrast are shown in Figs. 5 and 6. Here the two spheres are separated by the distance of $0.5a$. It is interesting to note that the effects of interaction remain quite strong in the case in which the centers of the spheres are on the Y axis. However, when the centers of the spheres are on a line perpendicular to the Y axis, the effects of interaction are almost negligible [Fig. 6(b)].

In Fig. 7 we show results for seven touching spherical inhomogeneities with radii $a = 0.1L$ located as described in the figure caption and illustrated in the inset. Note that the convergence in this case is reached for $l_{max} = 2$, which is, again, close to the value of the diffraction parameter of an isolated sphere ($x \approx 2.5$). At the same time, effects of the intersphere multiple scattering remain quite strong.

Results shown in Figs. 3–7 were obtained for strongly absorbing inhomogeneities with the contrast of the absorption coefficient (with respect to the background) of 16. The problem in this case is strongly nonlinear, and the Born approximation is inade-

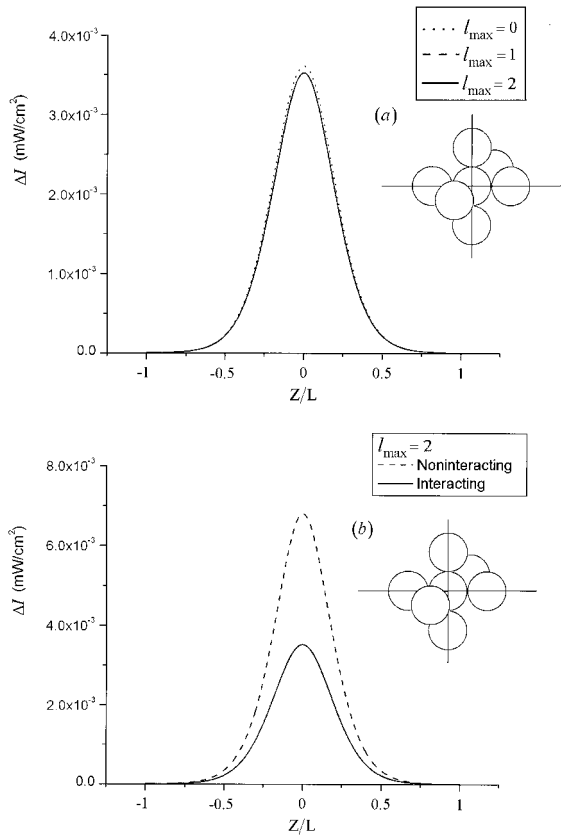

Fig. 7. Same as in Fig. 3 but for seven touching spheres with radii $a = 0.1L$ and centers at (0, 0.5L, 0), (0, 0.5L, 0.2L), (0, 0.5, −0.2L), (0, 0.3L, 0), (0, 0.7L, 0), (0.2L, 0.5L, 0), and (−0.2L, 0.5L, 0) and $k_i = 4\bar{k}$, $i = 1, \ldots, 7$. (The curves $l_{max} = 1$ and $l_{max} = 2$ in the top panel are indistinguishable.)

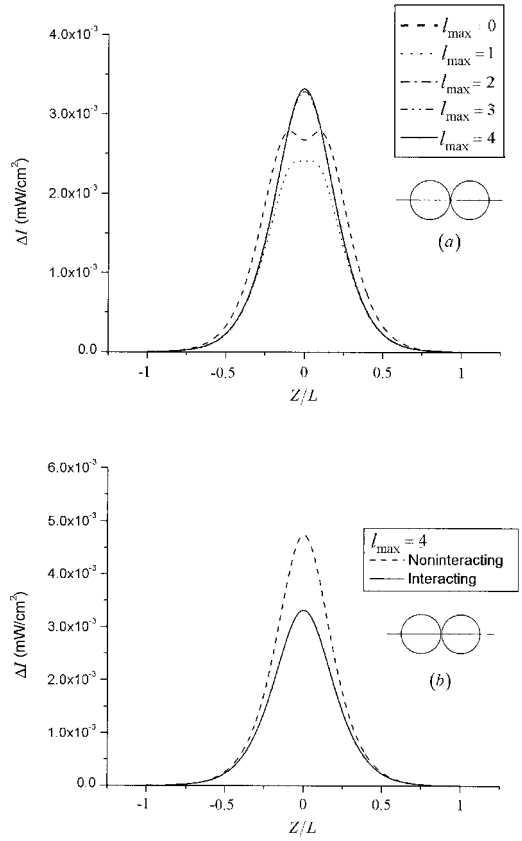

Fig. 8. Same as in Fig. 3 but for a smaller contrast: $k_1 = k_2 = 2\bar{k}$.

quate. In particular, multiple scattering of diffuse waves between different spheres is important, as can be seen from Figs. 3(b), 5(b), and 7(b). Although these examples are intended to illustrate the power of the developed method in a somewhat extreme case, the above contrast of the absorption coefficient is rarely encountered in practical situations. Therefore we have also performed simulations for a more realistic value of the contrast. Namely, we have repeated simulations whose results are shown in Figs. 3 and 4 with the same parameters, except that the contrast of the absorption coefficient was reduced and set to $\alpha_i = 4\bar{\alpha}\ \forall\ i$. The corresponding contrast of the diffuse wave number is $k_i = 2\bar{k}\ \forall\ i$. The results are shown in Figs. 8 and 9. It can be seen that, in the case of smaller contrast, convergence with l_{max} is achieved faster. This is quite evident in the case in which the sphere centers are on a line perpendicular to the measurement surfaces [e.g., compare Figs. 3(a) and 8(a)]. In particular, in the case in which $k_i = 2\bar{k}$ $\forall\ i$, the data function converges for $l_{max} = 3$ and is strictly positive even for smaller l_{max}. When the sphere centers are on a line parallel to the measurement surface, the dipole approximation $l_{max} = 1$ is quite accurate for both values of contrast [see Figs. 4(a) and 9(a)].

4. Diffuse–Nondiffuse Interfaces

The practical implementation of diffusion tomography imaging often requires placing the imaged medium in a chamber filled with index-matching fluid. The diffusion equation (4) may be used only inside the imaging chamber. As a result, in addition to the boundary conditions on the surfaces of discontinuity inside the turbid medium (diffuse–diffuse interfaces), we need to take into account boundary conditions on the imaging surfaces (diffuse–nondiffuse interfaces). The theoretical approach developed above can be easily generalized to include purely absorbing and purely reflecting infinite planar diffuse–nondiffuse interfaces. The purely absorbing boundary conditions are formulated as $u|_{\mathbf{r}\in\text{boundary}} = 0$, whereas the purely reflecting boundary conditions are $\hat{\mathbf{n}} \cdot \nabla u|_{\mathbf{r}\in\text{boundary}} = 0$, where $\hat{\mathbf{n}}$ is a unit vector normal to the boundary surface. The infinite planar interfaces appear in the half-space or slab imaging geometries.[13] Expressions for the physically measurable data function in the case in which the sources and detectors of diffuse radiation are located close to diffuse–nondiffuse interfaces are given in Ref. 26.

Accounting for the additional boundary conditions can be done with the method of images. The case of a single planar interface is illustrated in Fig. 10. Here the turbid medium, the source, and the spherical inhomogeneities are located in the right half-

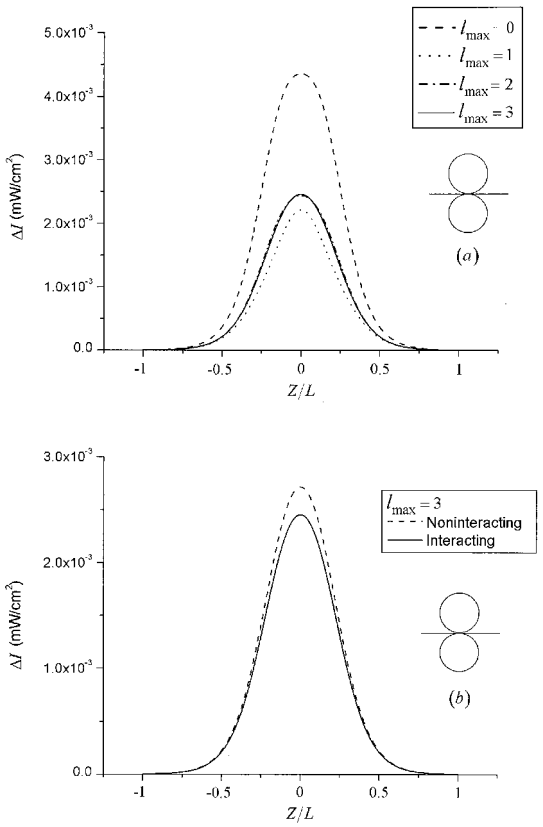

Fig. 9. Same as in Fig. 4 but for a smaller contrast: $k_1 = k_2 = 2\bar{k}$.

space. The mirror images of the inhomogeneities and the source are placed in the left half-space. The problem of finding the solution to Eq. (4) in the right half-space that satisfies either absorbing or reflecting boundary conditions on the surface $Y = 0$ is equivalent to finding the solution in the infinite space containing both the original and the image inhomogeneities and both the original and the image sources. (Of course, the obtained solution must be used only in the right half-space and has no physical meaning in the left half-space.)

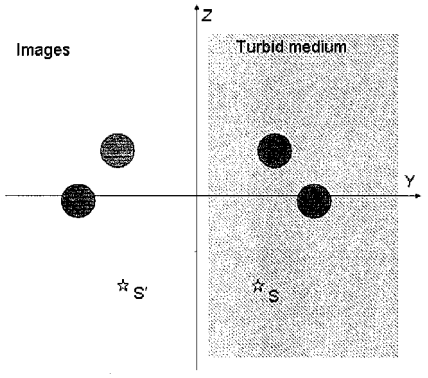

Fig. 10. Illustration of the method of images for the case of a single planar interface. The turbid medium, source, and spherical inhomogeneities are located in the right half-space. The mirror images of the inhomogeneities and source are in the left half-space.

Consider first purely absorbing boundaries. In this case, we take the optical constants of the image inhomogeneities to be the same as those of the original inhomogeneities and the amplitude (defined as the value of the constant A) of the image source to be the same in absolute value as that of the original source but negative. One must keep in mind that in the cw case there are no physical sources with negative amplitudes (in the case of a finite modulation frequency, the negative amplitude of the image source is equivalent to the relative phase shift of π with respect to the original source). However, such sources can be formally introduced in Eq. (4). Next, we solve Eq. (4) in the infinite space, taking into account the interaction of the original and the image spheres, as described in Section 2. The solution with the two sources is given simply by a superposition of the solutions obtained for each source separately. From the symmetry of the problem, it is easy to see that the value of u must turn to zero in the plane $Y = 0$. Thus the boundary conditions at the diffuse–nondiffuse interface are automatically fulfilled, and the boundary conditions on the surfaces of discontinuity in the right half-space are fulfilled by one's solving the system of Eqs. (22). Note that in the cw case the quantity u is purely real and strictly positive. It is easy to see that the positivity of u is not violated in the right half-space owing to the presence of a negative source in the left half-space. From the symmetry of the problem, the obtained u will be strictly negative in the left half-space, but, as mentioned above, the solution has no physical meaning in that region.

In the case of reflecting boundaries, the image source has exactly the same (positive) amplitude as the original source. Otherwise, the problem is solved exactly as in the case of absorbing boundaries. Finally, in the case of a slab (two parallel diffuse–nondiffuse interfaces), an infinite number of images (of both the sources and the inhomogeneities) are generated. However, the image sources and inhomogeneities that are sufficiently far from the measurement surfaces may be neglected owing to the exponential decay of diffusing waves, and the calculations can be approximately carried out for a finite system.

5. Summary and Conclusions

We have presented an approach for accurate modeling of multiple scattering of diffuse waves from several spherical inhomogeneities. The method has demonstrated excellent convergence properties even in the case in which the spherical inhomogeneities are of high contrast with respect to the background and touching. The number of linear equations that must be solved to obtain the scattering coefficients scales as $N(l_{max} + 1)^2$, where N is the total number of the inhomogeneities and l_{max} is the maximum order of scalar spherical harmonics used in the expansion of the scattered field. We have found that it is sufficient to take $l_{max} = \max_i(x_i)$, where $x_i = k_i a_i$ is the diffraction parameter of the ith spherical inhomoge-

neity. For example, for absorbing inhomogeneities with an absorption coefficient contrast of 16 times (with respect to the background) and a radius of approximately 0.2 of the diffuse wavelength (1.2 cm for the parameters selected in the simulations), $x \approx 5$, and convergence is reached for $l_{\max} \approx 4$. Thus the forward solution can be easily obtained, for example, for ten spherical inhomogeneities, in which case the total number of equations that must be solved is only 360. This should be contrasted with the finite-difference or finite-element methods, for which the number of equations for the forward problems solved in Section 3 can easily be as large as 10^6.

References and Notes

1. D. A. Boas, D. H. Brooks, E. L. Miller, C. A. DiMarzio, M. Kilmer, R. J. Gaudette, and Q. Zhang, "Imaging the body with diffuse optical tomography," IEEE Signal Process. Mag. **18,** 57–75 (2001).
2. F. Natterer, *The Mathematics of Computerized Tomography* (Wiley, New York, 1986).
3. M. C. W. Van Rossum and Th. M. Nieuwenhuizen, "Multiple scattering of classical waves: microscopy, mesoscopy and diffusion," Rev. Mod. Phys. **71,** 313–371 (1999).
4. S. R. Arridge, "Optical tomography in medical imaging," Inverse Probl. **15,** R41–R93 (1999).
5. B. W. Pogue, T. O. McBride, U. L. Ostererg, and K. D. Paulsen, "Comparison of imaging geometries for diffuse optical tomography of tissue," Opt. Express **4,** 270–286 (1999), http://www.opticsexpress.org.
6. J. P. Culver, V. Ntziachristos, M. J. Holboke, and A. G. Yodh, "Optimization of optode arrangements for diffuse optical tomography: a singular-value analysis," Opt. Lett. **26,** 701–703 (2001).
7. T. Durduran, J. P. Culver, M. J. Holboke, X. D. Li, L. Zubkov, B. Chance, D. N. Pattanayak, and A. G. Yodh, "Algorithms for 3D localization and imaging using near-field diffraction tomography with diffuse light," Opt. Express **4,** 247–262 (1999), http://www.opticsexpress.org.
8. M. Braunstein and R. Y. Levine, "Three-dimensional tomographic reconstruction of an absorptive perturbation with diffuse photon density waves," J. Opt. Soc. Am. A **17,** 11–20 (2000).
9. V. A. Markel and J. C. Schotland, "Scanning paraxial optical tomography," Opt. Lett. **27,** 1123–1125 (2002).
10. V. A. Markel and J. C. Schotland, "Effects of sampling and limited data in optical tomography," Appl. Phys. Lett. **81,** 1180–1182 (2002).
11. J. C. Schotland and V. A. Markel, "Inverse scattering with diffusing waves," J. Opt. Soc. Am. A **18,** 2767–2777 (2001).
12. V. A. Markel and J. C. Schotland, "Inverse scattering for the diffusion equation with general boundary conditions," Phys. Rev. E **64,** R035601 (2001).
13. V. A. Markel, V. Mital, and J. C. Schotland, "Inverse problem in optical diffusion tomography. III. Inversion formulas and singular-value decomposition," J. Opt. Soc. Am. A **20,** 890–902 (2003).
14. D. A. Boas, M. A. O'Leary, B. Chance, and A. G. Yodh, "Scattering of diffusive photon density waves by spherical inhomogeneities within turbid media: analytic solution and applications," Proc. Natl. Acad. Sci. USA **19,** 4887–4891 (1994).
15. V. A. Markel, J. A. O'Sullivan, and J. C. Schotland, "Inverse problem in optical diffusion tomography. IV. Nonlinear inversion formulas," J. Opt. Soc. Am. A **20,** 903–912 (2003).
16. J. M. Gerardy and M. Ausloos, "Absorption spectrum of clusters of spheres from the general solution of Maxwell's equations," Phys. Rev. B **25,** 4204–4229 (1982).
17. D. W. Mackowski, "Calculation of total cross sections of multiple-sphere clusters," J. Opt. Soc. Am. A **11,** 2851–2861 (1994).
18. D. W. Mackowski, "Electrostatics analysis of radiative absorption by sphere clusters in the Rayleigh limit: application to soot particles," Appl. Opt. **34,** 3535–3545 (1995).
19. R. Fuchs and F. Claro, "Multipolar response of small metallic spheres: nonlocal theory," Phys. Rev. B **35,** 3722–3727 (1987).
20. A. Ishimaru, *Wave Propagation and Scattering in Random Media* (Academic, San Diego, 1978), Vol. 1.
21. W. C. Chew, *Waves and Fields in Inhomogeneous Media* (IEEE Press, New York, 1995), App. D.
22. This should be contrasted with the known fact that the Mie solution for isolated spheres converges for the maximum order of spherical harmonics approximately equal to x.[23]
23. C. F. Boren and P. R. Hafmen, *Absorption and Scattering of Light by Small Particles* (Wiley, New York, 1983).
24. J. E. Sansonetti and J. K. Furdyna, "Depolarization effects in arrays of spheres," Phys. Rev. B **22,** 2866–2874 (1980).
25. Owing to this reason, we also expect similarly fast convergence for the problem of multiple quantum-mechanical scattering from several piecewise-constant spherically symmetrical potentials.
26. V. A. Markel and J. C. Schotland, "Inverse problem in optical diffusion tomography. II. Role of boundary conditions," J. Opt. Soc. Am. A **19,** 558–566 (2002).